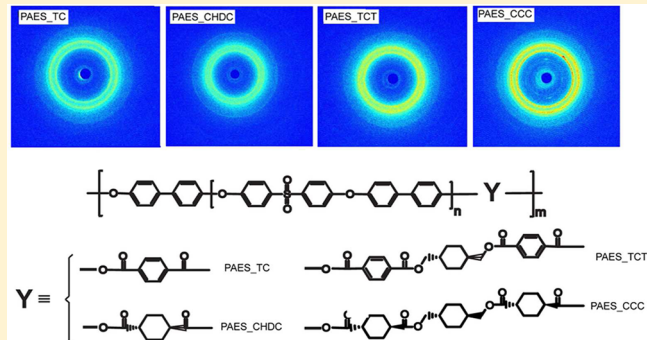


Crystallinity and Motional Dynamics Study of a Series of Poly(arylene ether sulfone) Segmented Copolymer Analogues

Bin Zhang,^{†,‡} Justin Spano,[†] Ying Chen,[†] Richard Turner,^{†,‡} and Sungsool Wi^{*,†}

[†]Department of Chemistry, and [‡]Macromolecules and Interfaces Institute, Virginia Polytechnic Institute and State University, Blacksburg, Virginia 24061, United States

S Supporting Information



1. INTRODUCTION

In order to continually develop novel synthetic polymeric materials and improve upon desired properties, it is crucial to utilize appropriate methods that successfully characterize these materials on the molecular level. One polymer system of industrial importance that has been highly researched is thermoplastic polyarylethers.^{1,2} In particular, poly(arylene ether sulfone)s (PAES) are known to have excellent thermal and mechanical properties.^{3,4} However, PAES copolymers possess limited applications due to their poor solvent resistance and unacceptable thermal dimensional changes near the glass transition temperature (T_g).

One way that these disadvantages can be addressed is by incorporating aliphatic segmental blocks, such as 1,4-cyclohexylene ring units, into the polymer backbone. It is well-known that incorporation of cyclohexylene rings into a sequence can enhance the mechanical properties and crystallization rate of the polymer system.⁵ Cyclohexylene ring containing polyesters, such as poly(1,4-cyclohexylenedimethylene 1,4-cyclohexanedicarboxylate) (PCCD), poly(butylene 1,4-cyclohexanedicarboxylate) (PBCHD), and poly(1,4-cyclohexane dimethylene terephthalate) (PCT), have been widely reported in the literature;⁶⁻⁸ however, to the best of our knowledge, little efforts have been done with cyclohexylene ring containing PAEs.

We have recently prepared a series of modified PAES copolymer sequences with short ester links for improving their

thermal and mechanical properties.⁹ Our current manuscript describes the investigation of the motional dynamics and correlation to the crystallinity of a series of PAES copolymer analogues that are modified with trans-1,4-cyclohexylene ring units. We employed solid-state NMR (SSNMR) spectroscopy to study the motional dynamics of the four differently modified PAES copolymers. Dynamic information of molecular motions whose time scales range from a few nanoseconds to milliseconds can conveniently be investigated by various types of SSNMR spectroscopic methods.^{10,11} In this work we sought to correlate molecular motions of various time scales with the conventional macroscopic properties, such as glass transition temperature (T_g), melting temperature (T_m), $\Delta T = T_m - T_g$, and crystallinity. These efforts may provide valuable information for understanding and controlling these copolymer materials, as SSNMR spectroscopy is capable of providing a wealth of complementary information to the conventional macroscopic characterization tools.¹¹

In this investigation we have employed the well-known proton spin-lattice (T_1)¹²⁻¹⁵ and rotating frame spin-lattice relaxation time ($T_{1\rho}$)¹³⁻¹⁷ SSNMR experiments. T_1 is affected by motions on the order of MHz regime, whereas $T_{1\rho}$ is sensitive to the

Received: April 14, 2012

Revised: June 13, 2012

Published: June 14, 2012

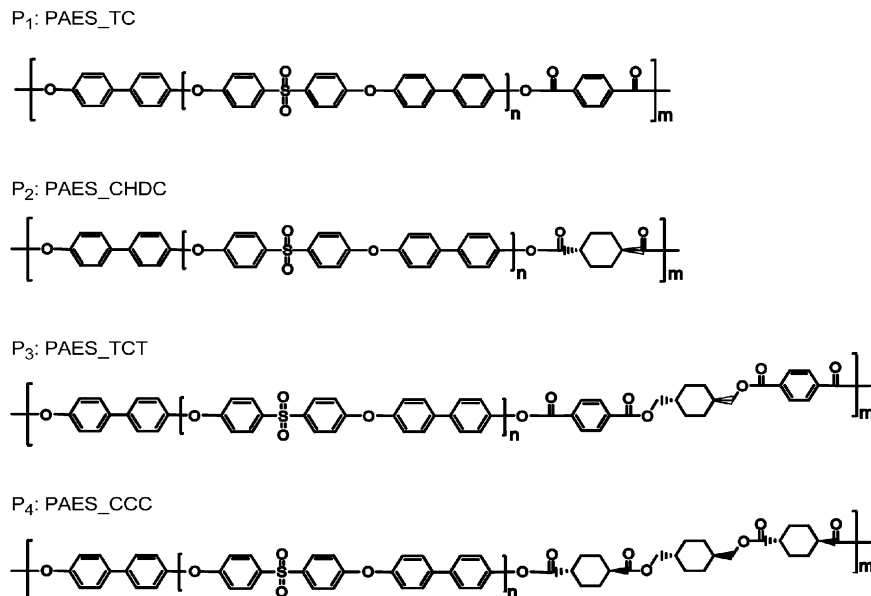


Figure 1. Structures of cyclohexylene ring containing PAES samples investigated (P₁, P₂, P₃, and P₄). The *n* and *m* values of each copolymer are 3 or 4.

dynamic processes on the order of kHz regime, so together these measurements help to understand the motions of polymer chains over a wide range of time scales from a few nanoseconds to microseconds. Also employed in our study were the two-dimensional phase adjusted spinning sideband (2D PASS)^{18,19} and the centerband-only detection of exchange (CODEX) experiments.^{20,21} The ¹³C CSA information obtained from 2D PASS experiment aids understanding not only the local electronic structures but the local mobility of molecular segments.^{18,19,22,23} The CODEX experiment is a powerful technique to investigate slow segmental reorientations of the polymer backbone ranging from a few seconds to a few milliseconds with a high sensitivity and resolution. The key information available from CODEX experiments are the amplitude and correlation time of segmental motions as well as, in some favorable cases, the geometry and number of exchanging sites involved in the motion.²⁰ These studies discussed herein provide insight on how different second monomers, aliphatic segmented blocks such as 1,4-cyclohexylene ring units, affect the mobility, packing, and crystallinity of the polymer chains, therefore, the thermal and mechanical properties of aromatic PAES copolymers.

2. EXPERIMENTAL SECTION

2.1. Polymer Synthesis. The detailed synthetic methods of the monomers, the hydroxyl-terminated PAES polymers with controlled molecular weight, and cyclohexylene ring containing PAES polymer are described in our previous paper.⁹ The structures of modified PAES block copolymers, incorporating aliphatic segments, investigated in this study are shown in Figure 1. The polymers are composed of biphenol based PAES oligomer components and ester components. Copolymer sequences incorporating terephthaloyl chloride (TC), *trans*-1,4-cyclohexane dicarbonyl dichloride (CHDC), *trans*-1,4-cyclohexane bis(methylene) bis(4-(chlorocarbonyl)benzoate) (TCT), and *trans*-1,4-cyclohexane bis(methylene) bis(4-(chlorocarbonyl)cyclohexane carboxylate) (CCC) monomers were named as P₁, P₂, P₃, and P₄, respectively. These block copolymers have the same “*n*” repeat unit, but differ in the “*m*” repeat unit; this *m*-block may contain cyclic alkyl groups (i.e., P₂ and P₄), aromatic

rings (i.e., P₁), or a combination of the two (i.e., P₃). The *n* and *m* values for each copolymer are 3–4.

2.2. Characterization of the Synthesized Polymer. The *T_g*'s and *T_m*'s of PAES copolymers were determined by differential scanning calorimetry (DSC) with a heating rate of 10 °C/min using a thermal analysis (TA) Q2000. Nitrogen was used as the carrying gas with a sample flow rate of 20 mL/min. *T_g*'s were determined in the second heating cycle of the experiment. Thermogravimetric analysis (TGA) was carried out by a TA Instrument, TGA 1000, by changing the temperature from 25 to 800 °C at a heating rate of 60 °C/min under nitrogen purging. Size exclusion chromatography (SEC) was used to determine molecular weights and molecular weight distributions. Chromatographic separations of PAES copolymers dissolved in SEC solvent (chloroform, *N,N*-dimethylformamide [DMF], and *N*-methyl-2-pyrrolidone [NMP]) were carried out on a Waters HR 0.5+ HR 2+ HR 3+ HR 4 styragel column set at 30 °C using the Waters Alliance model 2690 chromatograph. A Viscotek refractive index detector and a viscometer were used for molecular weight determination. Polystyrene standards were employed to construct a universal molecular weight calibration curve.

2.3. Solid-State NMR Spectroscopy. Polymer samples in powdered form were packed into 4 mm rotors for magic-angle-spinning (MAS) ¹³C SSNMR measurements using a Bruker Avance II-300 wide bore NMR spectrometer (7.05 T) operating at ¹³C and ¹H Larmor frequencies of 75.47 and 300.13 MHz, respectively.

¹H T₁ relaxation measurements were performed by employing an inversion recovery method;²⁴ a variable delay time *τ* following the initial ¹H 180° inversion pulse was combined with a ¹H–¹³C CP scheme, employing a short mixing time (~150 μs), to transfer ¹H magnetizations to the directly attached ¹³C atoms.²⁵ To measure ¹H T_{1ρ}, ¹H magnetizations created by a 90° pulse are spin-locked by a variable rf-pulse block that is 90° out of phase from the initial 90° pulse. A ¹H transverse magnetization under the spin-lock pulse undergoes signal decay with a relaxation parameter T_{1ρ}, which is sensitive over molecular motions in the time scale of a few microseconds regime.¹⁰ An indirect CP detection scheme with a short mixing time (~150 μs) was also

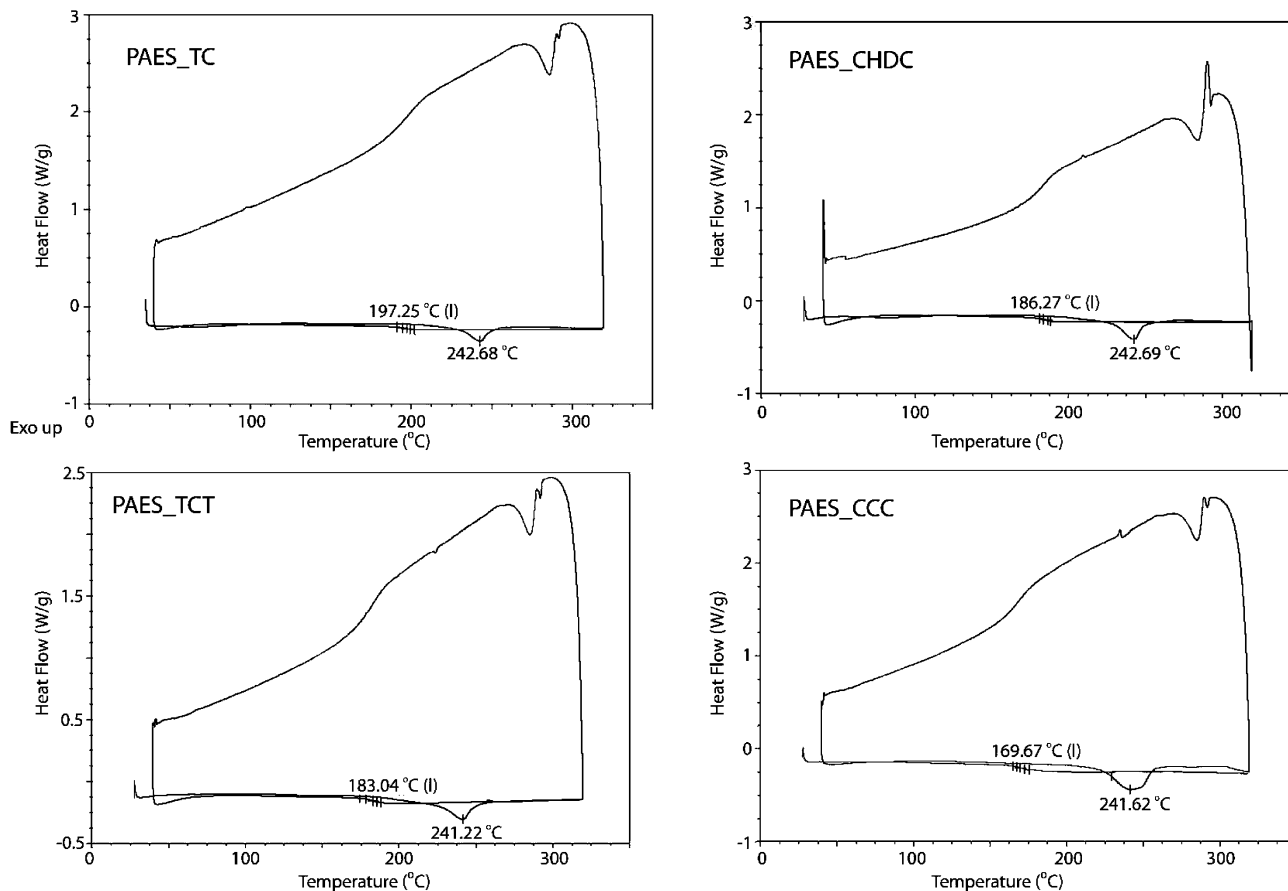


Figure 2. DSC curves of the biphenol based *trans*-1,4-cyclohexylene ring containing PAESs with the pseudointerfacial method (TA Q2000 heating rate 10 °C/min, cooling quench).

required for the $T_{1\rho}$ experiment.²⁵ For the ^1H T_1 and ^1H $T_{1\rho}$ measurements, the variable delay time and the variable spin-lock pulse duration were extended from 0 to 1 s in 10 increments of 0.1 s each (T_1) and from 0 to 10 ms in 10 increments of 1 ms each ($T_{1\rho}$). Relative intensities were found by comparing peak intensities for slices from the different delay times to the intensity of the first slice. Relaxation times were then extracted based on the linear regression of the experimental points in plots. The MAS spinning speeds for both ^1H T_1 and $T_{1\rho}$ experiments were 6.0 kHz.

The chemical shift anisotropy (CSA) of carbon sites was measured site-specifically by analyzing the spinning sideband patterns, which are separated by order, of a 2D PASS experiment^{18,19} employing a slow magic-angle spinning (MAS) condition (1.5 kHz). Successive rows of a 2D PASS spectrum were sheared along the indirect frequency domain so as to align all sidebands positioning at the same frequency position. A slice obtained at a specific frequency position provides the CSA sideband pattern of a ^{13}C site under investigation. Numerical simulations were carried out by employing a home-built program written by the Matlab programming language to extract CSA tensor parameters²⁶ from the experimental spectra.

The centerband-only detection of exchange (CODEX) experiment was used to probe the slow segmental reorientation of the copolymer backbone with time scales in the ranges of 1–3000 Hz in solids.^{20,21} The CODEX experiment has a special advantage in the signal sensitivity and resolution because it utilizes only the centerband of a MAS spectrum. The CODEX experiment monitors signals that diphase due to the segmental

reorientations of polymer chains that would induce changes in the orientation-dependent chemical shift frequencies. The MAS spinning speed employed in our CODEX experiments was 6.25 kHz.

All of these experiments utilize a ^{13}C -detection mode based on the Hartman-Hahn ^1H – ^{13}C cross-polarization (CP) scheme^{27,28} for obtaining enhanced signal intensity. The Hartman-Hahn ^1H – ^{13}C CP scheme utilizes a relatively short relaxation delay (2–5 s) that is governed by the shorter ^1H T_1 relaxation time rather than by the longer ^{13}C T_1 relaxation time. A pulse sequence known as the total suppression of spinning sidebands (TOSS)²⁹ that consists of a train of four π -pulses with appropriate delay times was combined with each of our NMR pulse sequences to obtain sideband free ^{13}C MAS spectra. The signal averaging was achieved by coadding 2048 scans with a 5 s acquisition delay time. ^1H and ^{13}C $\pi/2$ pulse lengths were 4 and 5 μs , respectively. Small phase incremental alternation with 64 steps (SPINAL-64)³⁰ decoupling sequence at 75 kHz power was used for proton decoupling during the direct ^{13}C signal detection in each experiment.

3. RESULTS AND DISCUSSION

3.1. Glass Transition and Melting Temperatures of PAES Analogues. Shown in Figure 2 are DSC curves revealing the T_m 's and T_g 's of biphenol based *trans*-1,4-cyclohexylene ring containing PAES oligomers (P_1 – P_4). In the presence of both aromatic biphenol and aliphatic *trans*-1,4-cyclohexylene ring blocks, both T_g and T_m were clearly observed in DSC curves. T_m 's of all P_1 – P_4 samples are virtually invariant although T_g 's are

changed as the flexibility of the aliphatic blocks increases. Being independent of the acid chloride monomers, the melting transitions of the P_1 – P_4 were all in the vicinity of 240 °C, whereas the glass transition temperatures are decreasing in the order of 200 °C (P_1) > 186 °C (P_2) > 177 °C (P_3) > 167 °C (P_4). Table 1 summarizes thus obtained T_g and T_m data of P_1 – P_4 .

Table 1. Molecular Weight, Glass Transition Temperature (T_g), Melting Temperature (T_m), and Enthalpy of Melting (ΔH_m) of a Series of Poly(arylene ether sulfone) Segmented Oligomers

	molar mass		polydispersity		T_g (°C)	T_m (°C)	ΔT (°C)	ΔH_m (J/g)
	M_n	M_w	M_w/M_n					
P_1	6.2k	9.2k	1.5	200	247	47	16.6	
P_2	5.2k	8.4k	1.6	186	244	58	26.1	
P_3	14.0k	19.3k	1.4	177	241	64	26.3	
P_4	12.2k	15.9k	1.3	167	244	77	41.3	

samples. Because of the structural independency of the melting transition, the observed decrease in T_g makes the crystallization window, which is defined as $\Delta T = T_m - T_g$, larger. The observed ΔT showed a clear trend, $P_4 > P_3 > P_2 > P_1$. The magnitude in ΔT can be correlated to the relative amount of crystallinity in the polymer matrix. A polymeric system with a bigger ΔT would produce a matrix with more crystalline regions because crystallization is determined by the rate of crystallization that is formed below T_m and the rate of the conformational motion of chains that is triggered above T_g . As the trans-1,4-cyclohexylene ring units introduced reduce the T_g and become more conformationally flexible, polymeric chains would be more mobile conformationally for achieving better interchain packing order above the T_g . Thus, a polymeric system with a wider ΔT window would produce a polymeric matrix with more extended crystalline regions.

With the DSC curves (Figure 2), the enthalpy of melting (ΔH_m) was calculated based on the integral area of the melting transition. ΔH_m values obtained are 16.6, 26.1, 26.3, and 41.3 J/g for P_1 , P_2 , P_3 , and P_4 , respectively (Table 1). The relative magnitude of ΔH_m observed is in the order of $P_4 > P_3 \geq P_2 > P_1$, reflecting qualitatively the relative amount of crystalline regions in the solid matrices. It is not possible to directly calculate the percentage of the crystalline regions from the experimental ΔH_m data for these polymers because biphenol based PAES polymers may or may not participate in the crystallization. However, simple comparison can be made with other semicrystalline polymers that have similar structures. The enthalpy of fusion of polyethylene terephthalate is 140 J/g, the enthalpy of fusion of polybutylene terephthalate is 145 J/g, and the enthalpy of fusion

of polyetheretherketone is 130 J/g (with a percentage of crystallinity of 30–35%).^{31,32} Compared to those semicrystalline polymers, the biphenol based *trans*-1,4-cyclohexylene ring containing PAESs obtained by the pseudointerfacial method exhibited low percentage of crystallinity in the solid matrix. The presence of the crystalline regions in our samples was also confirmed by wide-angle X-ray diffraction (WAXD) experiments. Crystallinity was identified in all types of biphenol based PAES polymers as shown in Figure 3. All four samples showed a similar WAXD pattern, exhibiting the semicrystalline nature of these polymers.

3.2. ^{13}C CPMAS Spectra of Polymer Samples. The ^{13}C spectra of the PAES copolymers investigated in this study are shown in Figure 4. In the experiments mentioned herein,

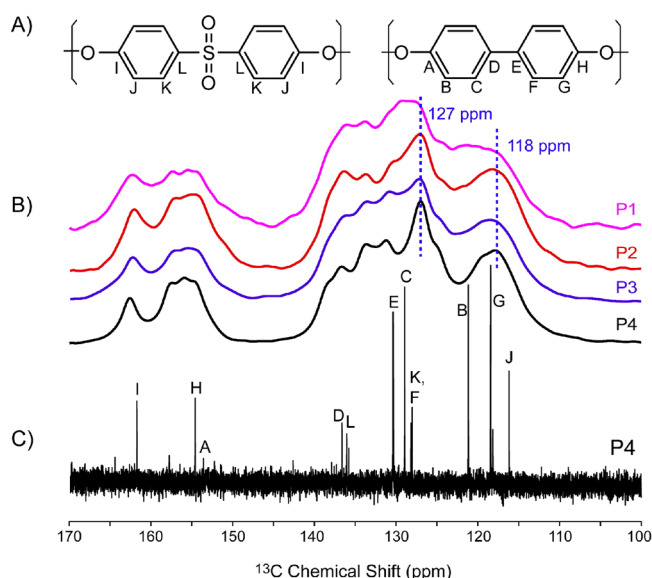


Figure 4. Details of NMR peak assignments. The aromatic segments from the polymers focused on in our ssNMR experiments are exhibited, with different ^{13}C sites labeled by letters (A). Example ^{13}C MAS spectra for each of the polymer samples (B) are shown atop a solution ^{13}C spectrum of P_4 (C). The letter-labeled peaks in the solution spectrum (C) correspond to the ^{13}C sites of the aromatic rings (A). Dashed vertical lines in B represent frequency positions employed for T_1 , $T_{1\rho}$, CODEX, and CSA experiments and show how the broad peaks in the MAS spectra at 127 and 118 ppm match up to the peaks in the solution spectrum. Additionally, a quaternary peak located at position H (136 ppm) is considered for CODEX experiments.

methine groups in the aromatic phenylene rings indicated at B, C, F, G, J, and K sites (Figure 4A) were utilized for various types of SSNMR experiments for monitoring molecular motions. Shown below the ^{13}C MAS spectra of P_1 – P_4 (Figure 4B) is a solution

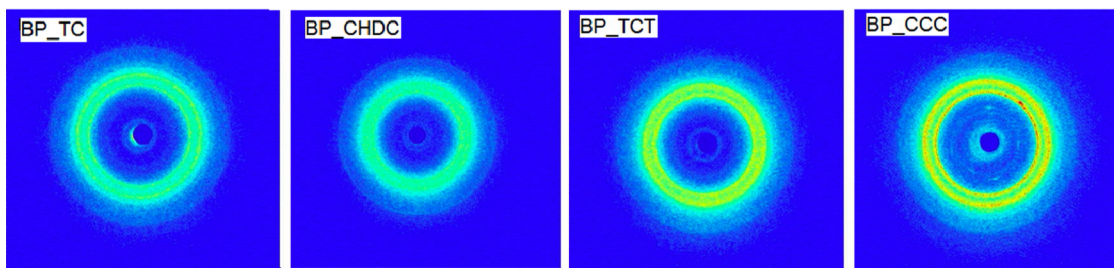


Figure 3. WAXD patterns of biphenol based *trans*-1,4-cyclohexylene ring containing PAESs with the pseudointerfacial method.

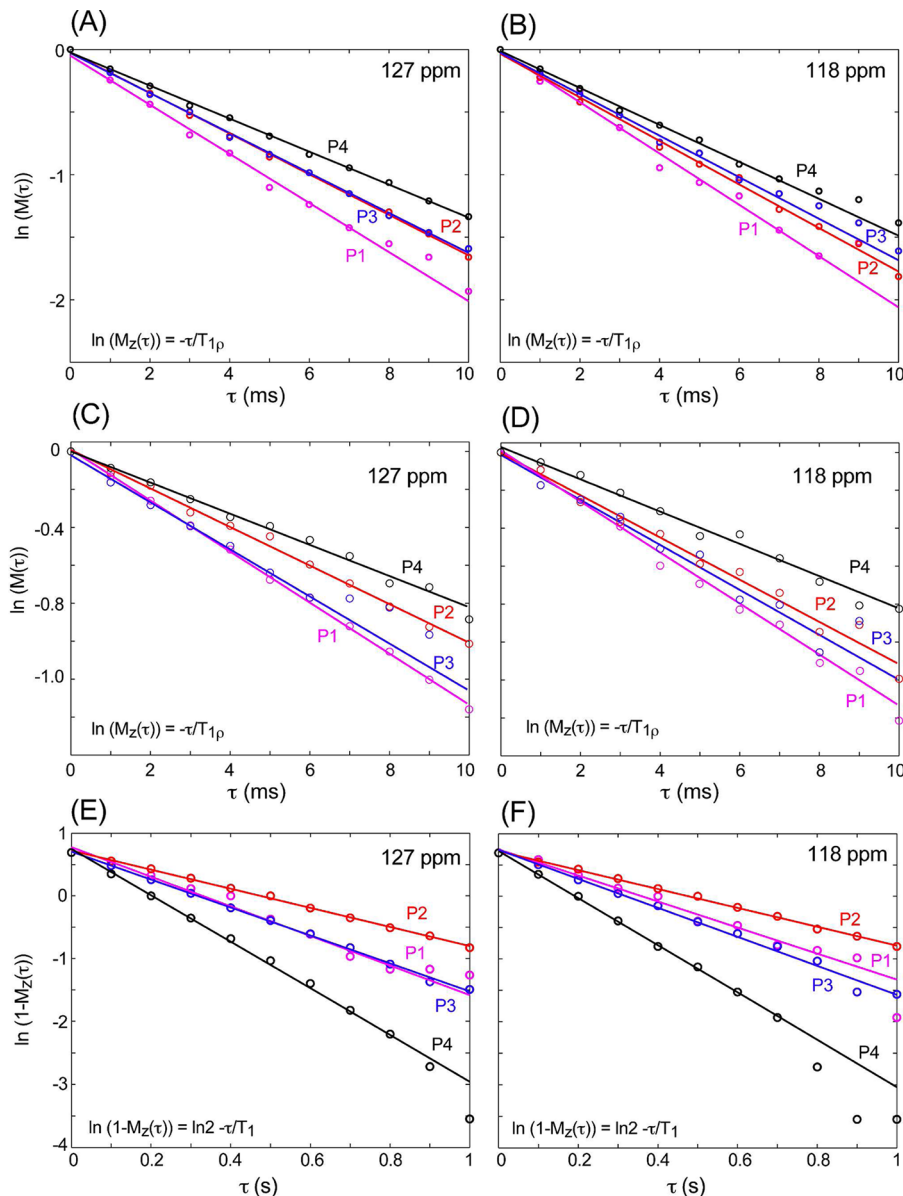


Figure 5. Least-square best-fit plots for ^1H $T_{1\rho}$ (A and B, $\omega_1 = 63$ kHz; C and D, $\omega_1 = 100$ kHz) and ^1H T_1 (E and F) relaxation time measurements on the four polymer samples, focusing on ^{13}C ssNMR signals at 127 (A, C, and E) and 118 ppm (B, D, and F). The experimental data shown as open circles and the best-fit results shown as solid lines are overlaid; these are color coded to represent P₁ (pink), P₂ (red), P₃ (blue), and P₄ (black). In the T_1 and $T_{1\rho}$ curves in panels A–F, initial data points in earlier mixing time have been focused for data fitting. Points deviated from the fitting curves at longer mixing time may suggest some nonlinear behavior of the each system.

^{13}C NMR spectrum of P₄ (Figure 4C) for guiding peak assignments. The solution-state ^{13}C NMR spectrum had been assigned for sites A–L and served to aid in assigning peaks in the SSNMR spectra. The ^{13}C SSNMR peaks centered at 127 and 118 ppm were chosen for analysis since these peaks correspond to the aromatic methine ^{13}C sites in phenylene rings: C, F, and K (127 ppm) and B, G, and J (118 ppm). Sites B, G, and J correspond to ^{13}C sites that are adjacent to the ^{13}C that is directly bonded to oxygen. Sites C and F are three bonds away from the ether oxygen, and site K is adjacent to the ^{13}C that is directly bonded to the sulfone group.

Signal overlaps due to the convolution of several peaks in the frequency regions of 127 and 118 ppm may prevent site-resolved SSNMR data interpretation. In many cases, however, this potential limitation can be lifted or, at least, alleviated in a multidimensional correlation spectroscopy or in a technique that

does not necessitate a fully resolved 1D spectrum. For instance, a fully resolved, site-specific NMR spectrum is not a prerequisite for measuring ^1H T_1 relaxation time in solid state. Protons in a bulk hydrocarbon sample system in solid-state form an equilibrium state via forming a strong ^1H – ^1H dipolar coupling network. Therefore, protons involved in a common spin network share a uniform T_1 value, not necessitating the spectra of fully resolved peaks for ^1H T_1 measurements. In ^{13}C SSNMR spectroscopy, meaningful structural and/or motional dynamics information can also be obtained even from overlapped ^{13}C sites if spectra of samples possessing a similar type of structures are compared.

3.3. ^1H $T_{1\rho}$ and T_1 Relaxation Times. Figure 5 summarizes experimental data obtained from ^1H $T_{1\rho}$ (Figure 5, panels A and B, $\omega_1 = 63$ kHz; Figure 5, panels C and D, $\omega_1 = 100$ kHz, where ω_1 is the spin-locking pulse power) and ^1H T_1 (Figure 5, panels E

and F) relaxation experiments measured at room temperature. Displayed are color-coded experimental points (open circles) and linear fittings (solid lines) for P₁ (pink), P₂ (red), P₃ (blue), and P₄ (black), as detected at 127 (Figure 5A,C,E) and 118 ppm (Figure 5B,D,F), respectively. For extracting ¹H T_{1ρ} times according to the time frame of the spin-lock period, τ, we have fitted our data to a linear equation, ln(M_{xy}(τ)) = ln(M_{xy}(0)) - τ/T_{1ρ}, where M_{xy}(0) is the size of the spin-locked transverse magnetization at the initial point (i.e., immediately after the CP; normalized to 1) and M_{xy}(τ) is the transverse magnetization (either M_x or M_y) monitored after a spin-lock period. The slope of this equation, 1/T_{1ρ}, was obtained by the least-squares fits. Figure 5A–D shows the experimental data and least-squares fits of our ¹H T_{1ρ} relaxation measurements. The range of ¹H T_{1ρ}'s thus obtained is in the range of 5.3–7.2 ms at ω₁ = 63 kHz and 7.4–12 ms at ω₁ = 100 kHz, respectively, as listed in Table 2. As obtained

Table 2. ¹H T_{1ρ} Relaxation Times

polymer	T _{1ρ} (127 ppm, μs) ^a			T _{1ρ} (118 ppm, μs) ^a		
	ω ₁ = 63 kHz	ω ₁ = 100 kHz	τ _c (μs)	ω ₁ = 63 kHz	ω ₁ = 100 kHz	τ _c (μs)
P ₁	5.1	7.4	5.1	4.9	7.4	5.6
P ₂	6.2	9.8	6.2	5.8	9.0	5.9
P ₃	6.3	8.1	3.8	6.0	8.4	4.7
P ₄	7.2	12	7.2	6.8	12	7.6

^athe range of error in T_{1ρ} data is ±0.1 μs.

from these fitting results, introduction of aliphatic blocks to the copolymer structure had resulted in increasing T_{1ρ} relaxation times for both ω₁ values. A polymeric sample system with an increased ΔT, which produces increased crystallinity in the polymer matrix, provides increased molecular packing order that, in turn, increases the T_{1ρ} time because segmental rotations or translations become less favorable under a tightly packed environment. Segmental rotations or translations of polymer chains within a few microseconds range become slower as the aliphatic segment blocks become longer and sterically more hindered. The magnitude of the observed ¹H T_{1ρ} relaxation times increases in the order of P₄ (CCC) > P₃ (CHDC) ≥ P₂ (TCT) > P₁ (TC) at both ω₁'s. Interestingly, the T_{1ρ} trend is also the trends of ΔT and ΔH_m observed (Table 1).

T_{1ρ} relaxation mechanism may reflect the segmental motions in the polymer chains that move in the frequency range of a few tenths or hundreds kHz regime (τ_c = 10⁻³–10⁻⁶ s).¹⁰ The ¹H T_{1ρ} relaxation times of P₁–P₄ samples would be governed by ¹H–¹H homonuclear dipolar coupling interactions because the contribution of proton's small chemical shift anisotropy (CSA) can be neglected. The contribution of ¹H–¹³C dipolar interactions is also negligible because of the low natural abundance of ¹³C (~1%). If an on-resonance spin-lock pulse irradiation is assumed, the measured relaxation rate, 1/T_{1ρ}, can be related to the following equation:^{10,33}

$$\frac{1}{T_{1\rho}} = \frac{1}{2} \langle \delta_{\text{HH}} \rangle^2 \left[\frac{3\tau_c}{1 + 4\omega_1^2\tau_c^2} + \frac{5\tau_c}{1 + \omega_H^2\tau_c^2} + \frac{2\tau_c}{1 + 4\omega_H^2\tau_c^2} \right] \quad (1)$$

Here, ⟨δ_{HH}⟩ is an unknown, effective ¹H–¹H dipolar coupling strength experienced by the protons at the measurement site. Frequencies defined by ω₁ and ω_H are the radiofrequency field

strength of the spin-lock pulse (63 kHz and 100 kHz) and the Larmor frequency of ¹H (301 MHz), respectively. Given the two independently measured T_{1ρ} values measured at ω₁ = 63 and 100 kHz, we could utilize the Newton–Raphson algorithm³⁴ to find the solution of eq 1 to find τ_c by eliminating the common factor, ⟨δ_{HH}⟩. The ranges of thus extracted τ_cs from our T_{1ρ} data from ¹³C resonances at 127 and 118 ppm are 5.1–5.6, 5.9–6.2, 3.8–4.7, and 7.2–7.6 μs, for P₁, P₂, P₃, and P₄, respectively (Table 2).

The trend observed in τ_c's for both 127 and 118 ppm is slightly different from that of T_{1ρ} itself, resulting in the order P₄ > P₂ > P₁ > P₃ rather than P₄ > P₃ > P₂ > P₁. This difference is due to the difference in the observed ΔT_{1ρ} [T_{1ρ}(ω₁ = 100 kHz) – T_{1ρ}(ω₁ = 63 kHz)]. The observed magnitudes in ΔT_{1ρ} are P₄ (4.8 ms) > P₂ (3.6 ms) > P₁ (2.3 ms) > P₃ (1.8 ms) at 127 ppm and P₄ (2.3 ms) > P₂ (3.6 ms) > P₁ (1.8 ms) > P₃ (4.8 ms) at 118 ppm. The correlation time τ_c extracted from T_{1ρ} becomes generally slower as the aliphatic segments included in *m*-block in the polymer sequence become longer and more tightly organized in the polymer matrix. This means that an increased amount of crystallinity in the polymer matrix would also increase intermolecular packing order, resulting in slower segmental rotations or translations of polymer chains. Our T_{1ρ} data exhibit an evidence that the time scale of the segmental motions of polymer chains within a few microseconds regime become slower as the flexibility of the polymer chain increases.

P₃, which demonstrates the biggest discrepancy between the trends in τ_c and T_{1ρ}, contains TCT, a mixed copolymer block of aromatic and aliphatic rings, as the *m*-block in the sequence (Figure 1). Thus, due to the unresolved nature of ¹³C SSNMR spectra in the aromatic region, ¹H T_{1ρ} data of methine protons in *n*-blocks of P₃ are contaminated by the motional characteristics of *m*-blocks. This signal contamination from *m*-blocks in the T_{1ρ} data of *n*-blocks may induce complications, obscuring the expected correlation to the ΔT data and, in turn, to the crystallinity data. The relatively weak peak intensities of aliphatic carbon sites, partly due to relatively scarce amount of aliphatic blocks in the polymer sequence and also the relatively difficult nature of complete ¹H–¹³C decoupling of aliphatic methylene groups, prevented us to measure T_{1ρ} of aliphatic protons.

As is clear in Figure 5D, T_{1ρ} data points observed in the longer mixing time deviate from the linearity, demonstrating potentially multiexponential components in the relaxation process. A signal contributed from both crystalline and amorphous regions may provide a multiexponential decay curve in T_{1ρ} relaxation. However, a short CP (~150 μs) mixing time would attenuate signal intensities transferred from protons from the amorphous domains. This is because the effective ¹³C–¹H dipolar coupling strength that is required for generating ¹³C CP signals is weaker in amorphous domains.

Crystalline regions would possess increased intermolecular packing order than amorphous regions in the solid matrix. In turn, increased crystalline regions would reinforce intermolecular ¹H–¹H interactions. T_{1ρ} relaxation is mainly governed by intra- or interchain associations and is sensitive over molecular motions that occur within a few nanometers scale around a site being investigated,¹⁰ a more localized probe than ¹H T₁ time that will be discussed later.

For extracting ¹H T₁ relaxation time the longitudinal magnetization M_z(τ) at time τ after the 180° inversion pulse must be related to the equilibrium magnetization M₀, which is normalized to be 1, by ln[M₀ – M_z(τ)] = ln[M₀ – M_z(0)] – t/T₁, where M_z(0), the magnetization right after the 180° inversion pulse, is adjusted to –1, ln designates a natural logarithm, and T₁

is the spin-lattice relaxation time. Then, a plot of $\ln(1 - M_z(\tau))$ as a function of τ (Figure 5E,F) gives a straight line with a slope $-1/T_1$ and an intercept $\ln 2$. The resultant ^1H T_1 values for P_1 – P_4 extracted from ^{13}C peaks at 127 and 118 ppm are summarized in Table 3. The ^1H T_1 times obtained from 127 ppm and 118

coupled network via forming strong ^1H – ^1H dipolar interactions. In addition to the self-relaxations, cross-relaxations among different ^1H spins would be facilitated by ^1H – ^1H dipolar interactions, resulting in an identical T_1 value by sharing magnetizations among different ^1H spins.

The trend observed in T_1 is roughly the opposite to that of $T_{1\rho}$. The T_1 time of P_4 is the shortest (0.27 s), those for P_1 and P_3 are intermediate and similar (0.42–0.48 s), and that of P_2 is the longest (0.66 s). Contrary to the $T_{1\rho}$ case, in which segmental rotations or translations associated with the $T_{1\rho}$ mechanism possess frequencies in the range of a few tenths or hundreds kHz regime, faster segmental motions involving atoms or smaller molecular segments spanning over a few atoms or bonds with frequencies that are close to the Larmor frequency of proton are responsible for the T_1 relaxation mechanism.¹⁰ Thus, the correlation times of these motional modes involving small

Table 3. ^1H T_1 Relaxation Times

	P_1	P_2	P_3	P_4
^1H T_1 (127 ppm, s) ^{a,b}	0.42	0.66	0.45	0.27
^1H T_1 (118 ppm, s) ^a	0.48	0.66	0.43	0.27

^a ^1H T_1 relaxation times are detected indirectly via ^{13}C peaks at 127 and 118 ppm. ^bThe error bound of T_1 measured is ± 0.01 s.

ppm are almost identical for a given sample, indicating that nearby protons in the polymer sequence form a strongly dipolar

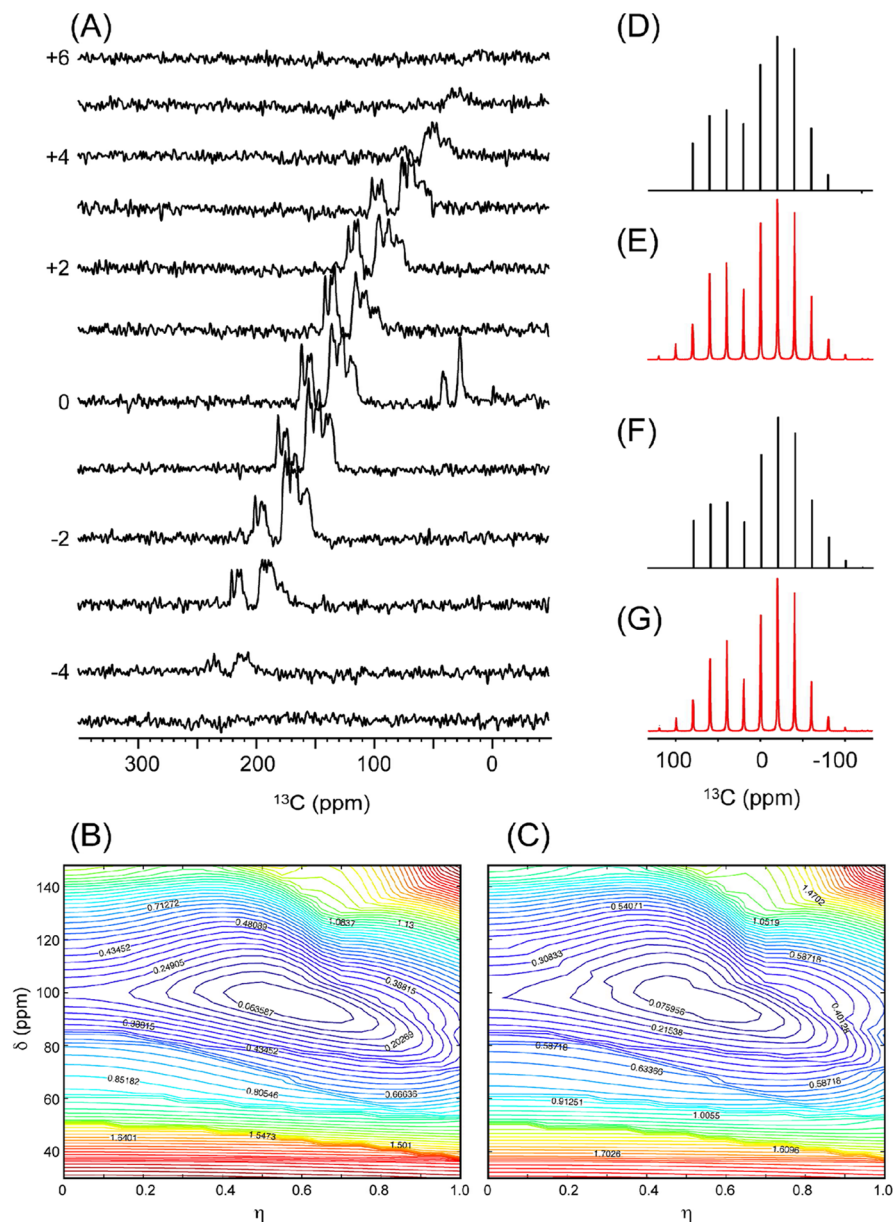


Figure 6. Two-dimensional ^{13}C PASS spectrum of P_2 (A). The ω_1 slices are sorted according to the order of the sidebands. The MAS spinning speed used was 1500 Hz. rms statistic as a function of the CSA parameters δ and η of P_2 (B) and P_4 (C) that are measured on the ^{13}C peak at 127 ppm. Experimental (D and F) and simulated (E and G) CSA spinning sideband bars obtained for P_2 (D and E) and P_4 (F and G) are shown.

segments in the aromatic PAES blocks would be less influenced by presence of aliphatic blocks than those motions associated with $T_{1\rho}$.

The observed T_1 trend would rather reflect the strength of effective dipolar coupling that is strongly influenced by the extent of crystallization. A polymer matrix with increased crystalline regions due to the presence of an extended ΔT range would possess stronger $^1\text{H}-^1\text{H}$ homonuclear dipolar interactions. Since the proton T_1 relaxation mechanism would be determined by $^1\text{H}-^1\text{H}$ homonuclear dipolar interactions, an effective T_1 relaxation rate is provided by $1/T_1 = \langle \mu_{\text{HH}} \rangle^2 \{ \tau_c / [1 + (\omega_0 \tau_c)^2] + 4\tau_c / [1 + (2\omega_0 \tau_c)^2] \}$,¹⁰ where ω_0 , μ_{HH} , and τ_c are the Larmor frequency of ^1H , mean effective $^1\text{H}-^1\text{H}$ dipolar coupling strength, and the motional correlation time, respectively. If the correlation time τ_c of the segmental rotations of small molecular fragments measured on the aromatic m -blocks is marginally variant on the modifications in the n -blocks, a polymer matrix with an enhanced crystallinity that provides a stronger effective $^1\text{H}-^1\text{H}$ dipolar coupling strength, $\langle \mu_{\text{HH}} \rangle$, will dominate the T_1 relaxation mechanism and produce a shorter ^1H T_1 time. Thus, the P_4 's shortest T_1 value is understandable because it has the biggest ΔT , thus the largest crystallinity in the polymer matrix. Stronger $^1\text{H}-^1\text{H}$ dipolar interactions due to the increased crystallization in the polymer matrix would mediate longer ranges of magnetization transfer among protons via cross-relaxations. Thus, a general trend obtained is that as we incorporate a more conformationally flexible aliphatic copolymer block into the copolymer sequence, the resultant polymer matrix provides a wider range in ΔT window, increased crystallinity, an increased effective $^1\text{H}-^1\text{H}$ dipolar interaction, and a shorter ^1H T_1 time.

The observed ^1H T_1 times however do not demonstrate an exact correlation to the observed ΔT 's ($\Delta T = T_m - T_g$) measured on P_1-P_4 samples. The observed ΔT 's increased in the order of P_1 (TC) < P_2 (CHDC) < P_3 (TCT) < P_4 (CCC) (Table 1), however, the T_1 relaxation rate ($R_1 = 1/T_1$) increased in the order of P_2 (CHDC) < P_1 (TC) \approx P_3 (TCT) < P_4 (CCC) (Table 3). This discrepancy can be explained by two competing factors that can influence the ^1H T_1 relaxation rate. The first factor is the chain flexibility of polymers that influences the crystallinity by decreasing the T_g of polymer matrix as we have discussed. The second competing factor would be the shape and/or symmetry of molecular segments that would influence the chain packing order of the polymer matrix.³⁵ The TC monomer, which consists of a pure aromatic phenylene ring, gave highest T_g because it does not possess any aliphatic structures. As the *trans*-1,4-cyclohexylene has been incorporated into the copolymer sequence, a decreasing trend in T_g was found as expected. However, it is interesting to notice that a longer T_1 time (slower the relaxation rate R_1) is actually observed from P_2 rather than from P_1 . The carbon skeleton of P_1 and P_2 are very similar to each other except one possesses an aromatic phenylene ring (P_1) and the other an aliphatic cyclohexylene ring (P_2) in the m -block. Because the T_1 measurement was performed at the room temperature below its T_g , the T_1 relaxation mechanism is affected by the chain flexibility effect and the packing improvement effect. Due to the linearity of the *trans*-1,4-cyclohexylene ring, it has been reported that it improves the chain packing order compared to the aromatic analogue.³⁶ The *trans*-1,4-cyclohexylene possesses more flexible conformational freedoms in the backbone compared to the aromatic analogue. However, the *trans*-1,4-cyclohexane dicarboxylate segment in P_2 takes only one energetically favorable conformational structure because the *trans*-1,4-cyclohexane

dicarboxylates would take dominantly a chair form with dicarboxylic substituents in equatorial positions at room temperature. When the TC and CHDC containing polymers are compared, the one containing CHDC possesses a more flexible aliphatic backbone, however the local segmental motion of the *trans*-1,4-cyclohexane dicarboxylates would be largely restricted by the strong packing improvement effect that may lead to a smaller T_1 value. In the case of TCT, the two factors balanced out, resulting in a similar T_1 value to the TC polymer. When three continuous *trans*-1,4-cyclohexylene rings were incorporated in the monomer CCC, the chain flexibility becomes the main effect and ends up with the smallest T_1 value. Interestingly, the actual trend observed in ^1H T_1 times follows exactly the trend observed in the polydispersity (M_w/M_n) of samples. The magnitudes of the polydispersity (M_w/M_n) measured are in a trend $P_2 > P_1 > P_3 > P_4$ (Table 1).

3.4. Chemical Shift Anisotropy. Chemical shift anisotropies (CSAs) of ^{13}C sites in the PAES blocks were analyzed to investigate the influence of the segmented aliphatic blocks on the local electronic structures and motions. Shown in Figure 6A is, for example, the 2D PASS spectrum of P_2 . The central band and multiple spinning sidebands of each ^{13}C site in a 2D PASS spectrum are separated by the order along the indirect frequency domain in such a way that the frequency position of a spinning sideband is shifted by $\nu_r \times \text{SD}/\text{SW}$ from a band that is located a step below it, where SD, ν_r , and SW are the spectral data point, the spinning speed (1.5 kHz), and the spectral width of the spectrum, respectively. All of the central and sidebands from a ^{13}C site must be aligned at the same frequency position in the direct acquisition domain to extract a 1D projection for obtaining MAS sideband spectrum. For this purpose, a shearing transformation was applied to the 2D PASS spectrum shown in Figure 6A by shifting each row by $-k(\nu_r \times \text{SD}/\text{SW})$, where $k (= 1, 2, \dots)$ is the order of spinning sideband.

An experimental 1D MAS sideband pattern extracted from the sheared 2D PASS spectrum was normalized in such a way that the intensity of the biggest line was set to be 1 and the intensities of other lines were adjusted according to the relative intensity ratios with respect to the biggest line. Numerical simulations were carried out to find the best-fit spectrum and tensor parameters for each data set by employing a home-built program written in Matlab programming language. The root-mean-square variance, $(\sum (E_i - S_i)^2)^{1/2}$, where E_i and S_i are the line intensity of experimental and simulated 1D MAS spectra of order i , was calculated for each data point on a two-dimensional grid map formed by varying trial tensor parameters, δ and η . Figure 6, panels B (P_2) and C (P_4), are the contour maps, thus obtained, that show the calculated variances, considering the MAS sideband spectrum taken at 127 ppm of each 2D PASS spectrum.

Regions of the minimum variance are visible in both contour maps. The position of the minimum variance corresponds to the optimal δ and η parameters that provide the best-fit simulation. Panels D and F in Figure 6 are the experimental 1D MAS sideband spectra of P_2 and P_4 , respectively, that are taken at 127 ppm. Panels E and G in Figure 6 are the corresponding best-fit simulations of P_2 and P_4 , employing CSA tensor parameters found from panels B and C in Figure 6 ($\delta = 94 \pm 5$ ppm; $\eta = 0.6 \pm 0.1$). Table 4 summarizes CSA values of P_1-P_4 samples thus obtained from ^{13}C sites at 136 and 127 ppm. As can be seen in the table, the range of CSA tensor parameters obtained at the common block are all very similar, regardless of the type of segmented copolymer structures. This invariance implies that the changes in the intermolecular packing order, ultimately the

Table 4. CSA Parameters of ^{13}C Sites Measured on 136 and 127 ppm

peak position	P_1		P_2		P_3		P_4	
	δ^a	η^b	δ	η	δ	η	δ	η
136 ppm	88 ^c	0.7 ^d	88	0.6	90	0.6	92	0.5
127 ppm	92	0.5	94	0.6	88	0.6	94	0.6

^aThe CSA, δ , is defined by $\delta_{33} - \delta_{\text{iso}}$, where $\delta_{\text{iso}} = (\delta_{11} + \delta_{22} + \delta_{33})/3$. ^b δ_{ii} ($i = 1, 2$, or 3) is a tensor element defined in the principal axes frame (PAS). ^cThe asymmetry parameter η is $(\delta_{11} - \delta_{22})/\delta$. ^dThe error bound of CSA is ± 5 ppm.

crystallinity of the polymeric matrix, due to the introduction of aliphatic segments span over long distances involving a few adjacent segmented domains. The aromatic PAES segments may form local structural domains that are isolated from the aliphatic segments on the nanoscopic scale.

3.5. Slow Segmental Reorientation Dynamics. Figure 7 shows ^{13}C CODEX NMR data measured on P_1 (B–C) and P_4 (C–F) detected at 154, 127, and 34 ppm and the corresponding best-fit simulations to extract the correlation times of the slow reorientational dynamics of polymers. We have chosen only two extreme examples P_1 and P_4 to extract the influence of the aliphatic segmental blocks on the chain dynamics of aromatic PAES block. Demonstrated in Figure 7A are the pure exchange CODEX spectra ($\Delta S = S_0 - S$) of P_4 sample recorded at several exchange mixing times, t_m 's, under a fixed CSA recoupling time, $t_{\text{CSA}} = 0.32$ ms ($N = 4$; $t_{\text{CSA}} = 2\tau_r$). Peaks shown in the pure

exchange CODEX spectra are those ^{13}C sites that undergo conformational reorientations during the CODEX mixing time. Shown on the bottom of Figure 7A for comparison is the CPMAS spectrum that shows all the carbon sites regardless of the relative mobility of conformational reorientations. Plotted in Figure 7B–F are pure CODEX exchange signal intensities, $\Delta S = (S_0 - S)$, of P_1 and P_4 samples recorded at 154, 127, and 34 ppm that are normalized by S_0 , where S_0 is the signal intensity recorded by switching t_m and t_z in the CODEX pulse sequence to compensate signal loss due to the T_1 and T_2 relaxations. As the mixing time t_m increases, the spectral intensity of $\Delta S/S_0$ increases as expected.

Filled, red circles with error bars in each graph in Figure 7B–F were used to designate the experimental $\Delta S/S_0$ intensities recorded at 154 [B (P_1) and D (P_4); aromatic quaternary carbons], 127 [C (P_1) and E (P_4); aromatic methine sites], and 34 ppm [F (P_4); aliphatic carbon sites], respectively. Our experimental CODEX data were fitted to a stretched exponential function, $A[1 - \exp\{-t_m/(\tau_0)^{\beta}\}]$,³⁷ where A ($0 < A < 1$) is a value to which the $\Delta S/S_0$ signal intensity approaches asymptotically at a long mixing time and β and τ_0 are the stretched exponential coefficient and the center of the correlation time, respectively. The β coefficient is related to the width of the correlation time distribution.³⁸ Then, the mean correlation time, $\langle\tau_c\rangle$, for the segmental reorientational motion, for instance, of phenylene ring-flips is related to τ_0 and β values by $\langle\tau_c\rangle = (\tau_0/\beta)\Gamma(1/\beta)$,³⁷ where Γ is the gamma function. The mean

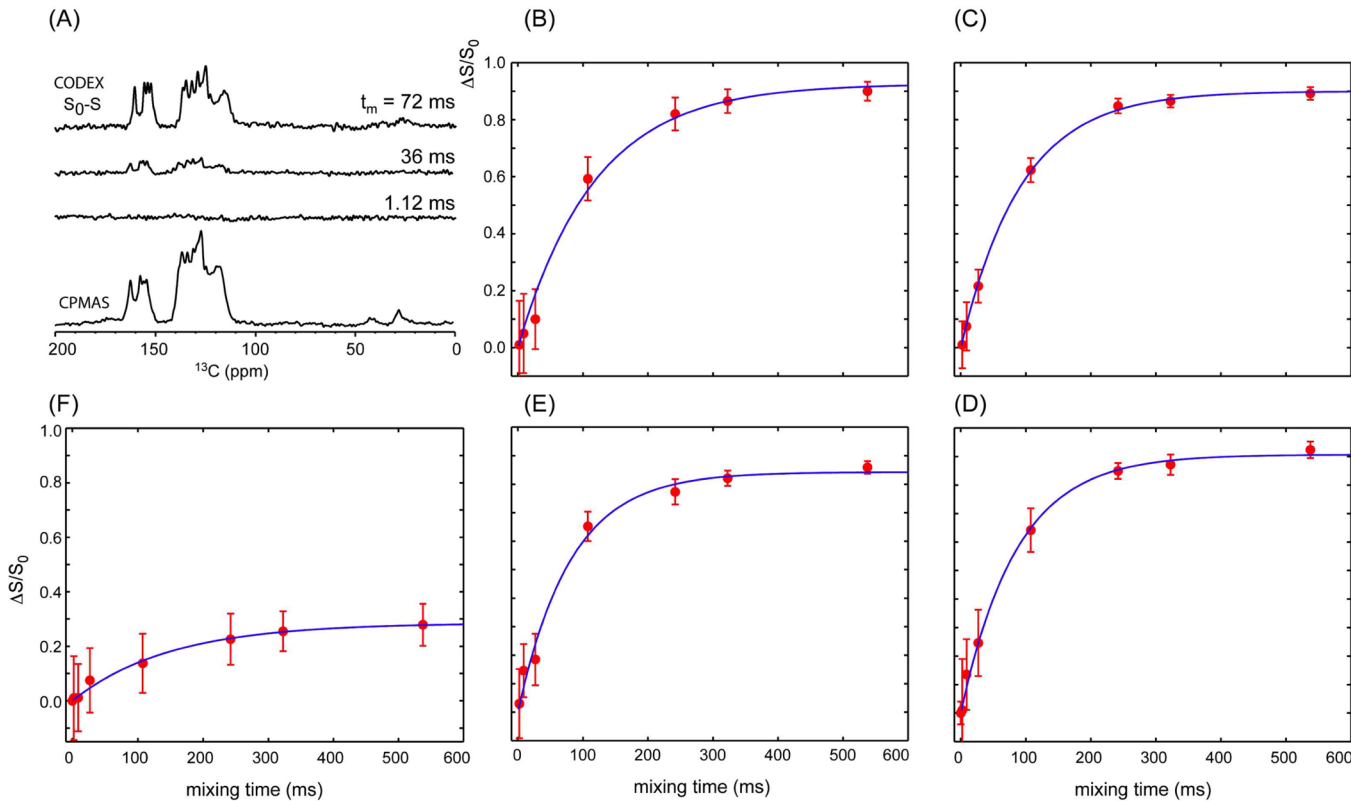


Figure 7. CODEX NMR data of P_1 and P_4 . Pure exchange CODEX spectra of P_4 (A) recorded by varying t_m with $t_{\text{CSA}} = 0.32$ ms and $t_z = 1.12$ ms. The normalized t_m -dependent CODEX dephasing intensities (B–C: P_1 and D–F: P_4) measured on the ^{13}C peaks at 154 (B and D), 127 (C and E), and 34 ppm (F). Error bars are obtained by calculating the signal-to-noise ratio (SINO) of both signal (S) and reference (S_0) spectra according to $\delta(S/S_0) = (S/S_0)[(1/SINO)_{S0} + (1/SINO)_S]$. Aromatic methine groups with (P_4) and without (P_1) aliphatic, segmented copolymer blocks demonstrate different motional correlation times in CODEX experiments. A long aliphatic, segmented copolymer block included in the common aromatic block has resulted in slower motional reorientations for both quaternary and methine carbon sites in the common aromatic segments.

Table 5. Mean Correlation Times and Stretched Exponential Coefficients Obtained from the t_m -Dependent CODEX Data

	P_1		P_4		
	154 ppm	127 ppm	154 ppm	127 ppm	34 ppm
A	0.877	0.891	0.925	0.844	0.37
τ_0 (ms)	102 \pm 3	90. \pm 3	91 \pm 3	81 \pm 3	385 \pm 20
β	1.40 \pm 0.05	1.07 \pm 0.05	0.904 \pm 0.02	0.990 \pm 0.02	0.72 \pm 0.10
$\langle \tau_c \rangle$ (ms)	93 \pm 3	88 \pm 3	95 \pm 3	82 \pm 3	475 \pm 20

correlation times and the stretched exponential coefficients thus obtained from the curve fitting are summarized in Table 5.

As can be seen in Table 5, the best-fit CODEX simulation data obtained employing the stretched exponential function model have provided a correlation time within the range of 82 (\pm 3) to \sim 88 (\pm 3) ms for the aromatic methine sites and virtually invariant values (93 [\pm 3] to \sim 95 [\pm 3] ms) for the aromatic quaternary carbon sites. Although the $\langle \tau_c \rangle$ values for the aromatic methine sites with and without aliphatic segmentation are not significantly different, the difference is at least beyond the error bound detected (\pm 3 ms), indicating that the aliphatic segmentation in the m -blocks speeds up the rotational reorientations of aromatic phenylene rings present in the n -blocks. Thus, an inclusion of the aliphatic blocks in the copolymer sequence had resulted in an increase in the rate of the segmental reorientation motion of aromatic methine site, while maintaining a virtually invariant rate for quaternary sites. This implies that an inclusion of the aliphatic, segmented block in the polymer sequence may have resulted in an overall increase of the free volume in the polymer matrix, making the ring-flip motions of aromatic rings more favorable. The correlation time of the aliphatic chain motions observed at 34 ppm of P_4 was much more slower (475 \pm 20 ms) than those of aromatic sites. The reorientational motion of aliphatic segments would be less favorable than the aromatic phenylene rings, which can undergo much easier ring-flip motions around the positions where they are located, because aliphatic segments would encounter more restrictions from the nearby chains against their reorientational rotations or translations. The slow reorientational dynamics of polymer chains would possess multiple motional modes with a distribution in the magnitude of correlation times because the inhomogeneous nature of the solid matrices include both crystalline and amorphous regions.

Another experimentally observed feature is that the line width of peaks in the CODEX spectra is narrower than those peaks in the CPMAS NMR spectrum (Figure 7A). This feature would be attributed to the difference in the relaxation times (both T_1 and T_2) of the amorphous and crystalline regions. The ^{13}C sites in the amorphous regions would possess shorter relaxation times. Therefore, ^{13}C signals in CODEX spectra are mainly from the crystalline regions in the polymer matrix because peaks from the amorphous regions might have undergone more signal decays during the periods of relatively long CODEX mixing times. As can be seen in Figure 7A, the pure exchange CODEX spectra are indeed sharper than the CPMAS spectrum, indicating that the motional characteristics revealed in the CODEX spectra are mainly from the crystalline domains in the polymer matrix.

4. CONCLUSION

As analyzed by DSC, WAXD, and SSNMR experiments, it has been demonstrated that the amount of crystallization in the solid matrix of PAES copolymer analogues was increased by incorporating aliphatic segmented blocks, such as *trans*-1,4-cyclohexylene rings, in the copolymer sequence. As confor-

tionally more flexible copolymer segments were incorporated into the aromatic PAES sequence, the resultant polymer matrix lowered T_g while maintaining a nonvariant T_m , thus increased the ΔT ($= T_m - T_g$). Aliphatic blocks with bigger ΔT , thus, with increased conformational freedom above T_g , enable accommodations of more favored conformational structures at temperatures above T_g , improving the packing order of the polymer matrix by increasing crystalline regions. A polymer system with a bigger ΔT window possesses a kinetically favorable condition for the polymer crystallization, which is determined by a balance between the rate of the crystallization below T_m and the motional dynamic rate of polymer chains above T_g . The enthalpy of melting (ΔH_m) that shows a direct correlation to the observed ΔT also increased as the chain flexibility effect of the segmented aliphatic blocks increased.

The observed $T_{1\rho}$ relaxation time becomes slower as the crystallinity of the sample has increased. $T_{1\rho}$ is sensitive to the intermolecular association of polymeric chains because the packing order as well as the interchain association in the polymer matrix would be increased if the crystallinity of the polymer matrix increases. A slower correlation time (τ_c) was observed for the chain motions of modified PAES copolymers associated with the $T_{1\rho}$ relaxation mechanism as the amount of crystallinity increases. Since P_3 possesses both aromatic and aliphatic rings in the m -block, the observed $T_{1\rho}$ time of P_3 may contain contributions from both n - and m -blocks, obscuring a clear correlation to the observed $T_{1\rho}$ times.

Fast motions such as segmental rotations or translations involving small atoms or small molecular segments that occur within a few nanoseconds would not be changed dramatically over the changes in the segment n of polymer sequence, maintaining a similar range of correlation times. Instead, the strengthened effective $^1\text{H}-^1\text{H}$ dipolar coupling strength, μ_{HH} , due to the formation of crystalline domains will dominate the relaxation mechanism by making the magnitude of T_1 relaxation time shorter. The observed order in the magnitude of ^1H T_1 relaxation time was also determined by a balanced effect between the chain flexibility and chain packing order. Compared to the pure aromatic polymer, P_1 , a chair structured *trans*-1,4-cyclohexylene ring is conformationally favored for increasing the chain-packing order, overcoming the chain flexibility effect.

Being measured on methine sites in aromatic phenylene rings, the slow reorientational motions of polymer chains that occur within a few milliseconds regime become slightly faster as the aliphatic segment blocks are introduced in the copolymer sequence. An increased conformational flexibility in the segmented m -block leads to an overall, shorter average correlation time throughout the entire polymer matrix. The increased conformational flexibility of the segmented blocks enables rotational reorientations of polymer chains more favorable and faster.

The CSA tensor parameters obtained at the common PAES block are invariant, regardless of the type of segmented copolymer structures. This invariance implies that the changes

in the crystallinity of the polymeric matrix do not change the local structural and motional environments of aromatic PAES blocks that are isolated from the aliphatic segments on the nanoscopic scale.

■ ASSOCIATED CONTENT

Supporting Information

¹H wide-line spectra. This material is available free of charge via the Internet at <http://pubs.acs.org>.

■ AUTHOR INFORMATION

Corresponding Author

*Tel: 540-231-3329. Fax: 540-231-3255. E-mail: sungsool@vt.edu.

Author Contributions

J.S. and B.Z. contributed equally to the present work.

Notes

The authors declare no competing financial interest.

■ ACKNOWLEDGMENTS

This work was supported by the Petroleum Research Fund (PRF #: 51622-ND7).

■ REFERENCES

- (1) Hale, W. F.; Farnham, A. G.; Johnson, R. N.; Clendinning, R. A. *J. Polym. Sci., Part A-1: Polym. Chem.* **1967**, *5*, 2399–2414.
- (2) Johnson, R. N.; Farnham, A. G.; Clendinning, R. A.; Hale, W. F.; Merriam, C. N. *J. Polym. Sci., Part A-1: Polym. Chem.* **1967**, *5*, 2375–2398.
- (3) Rose, J. B. *Polymer* **1974**, *15*, 456–465.
- (4) Robeson, L. M.; Farnham, A. G.; McGrath, J. E. *Appl. Polym. Symp.* **1975**, *1975*, 373–385.
- (5) Turner, S. R. *J. Polym. Sci., Part A-1: Polym. Chem.* **2004**, *42*, 5847–5852.
- (6) Corrado, B.; Annamaria, C.; Paola, M.; Elisabetta, M.; Giancarlo, B.; Francesco Di, C. *Macromol. Chem. Phys.* **2008**, *209*, 1333–1344.
- (7) Charles, J. K.; Alan, B.; James, G. S. *J. Polym. Sci., Part A: Gen. Pap.* **1964**, *2*, 2115–2125.
- (8) Scheirs, J.; Long, T. E. *Modern polyesters: chemistry and technology of polyesters and copolyesters*; John Wiley & Sons, Inc.: New York, 2003.
- (9) Zhang, B.; Turner, S. R. *J. Polym. Sci., Part A-1: Polym. Chem.* **2011**, *49*, 4316–4324.
- (10) Kimmich, R. *NMR Tomography, Diffusometry, Relaxometry*; Springer: Berlin, 1997.
- (11) Schmidt-Rohr, K.; Spiess, H. W. *Multidimensional Solid-State NMR and Polymers*; Academic Press: San Diego, 1994.
- (12) Kishore, A. I.; Herberstein, M. E.; Craig, C. L.; Separovic, F. *Biopolymers* **2002**, *61*, 287–297.
- (13) Wang, J.; Cheung, M. K.; Mi, Y. *Polymer* **2002**, *43*, 1357–1364.
- (14) Masson, J. F.; Manley, R. S. J. *Macromolecules* **1992**, *25*, 589–592.
- (15) Zhang, X.; Takegoshi, K.; Hikichi, K. *Macromolecules* **1992**, *25*, 2336–2340.
- (16) Simmons, A.; Natansohn, A. *Macromolecules* **1991**, *24*, 3651–3661.
- (17) Huijgen, T. P.; Gaur, H. A.; Weeding, T. L.; Jenneskens, L. W.; Schuurs, H. E. C.; Huysmans, W. G. B.; Veenman, W. S. *Macromolecules* **1990**, *23*, 3063–3068.
- (18) Antzutkin, O. N.; Shekar, S. C.; Levitt, M. H. *J. Magn. Reson. A* **1995**, *115*, 7–19.
- (19) Antzutkin, O. N.; Lee, Y. K.; Levitt, M. H. *J. Magn. Reson.* **1998**, *135*, 144–155.
- (20) deAzevedo, E. R.; Hu, W.-G.; Bonagamba, T. J.; Schmidt-Rohr, K. *J. Am. Chem. Soc.* **1999**, *121*, 8411–8412.
- (21) deAzevedo, E. R.; Hu, W.-G.; Tito J. Bonagamba, T. J.; Schmidt-Rohr, K. *J. Chem. Phys.* **2000**, *112*, 8988–9001.
- (22) Saitô, H.; Ando, I.; Ramamoorthy, A. *Prog. NMR Spec.* **2010**, *57*, 181–228.
- (23) Wei, Y.; Lee, D.-K.; Ramamoorthy, A. *J. Am. Chem. Soc.* **2001**, *123*, 6118–6126.
- (24) Harris, R. K. *Nuclear Magnetic Resonance Spectroscopy*; Pitman: London, 1983.
- (25) Lee, C. H.; Spano, J.; McGrath, J. E.; Cook, J.; Freeman, B. D.; Wi, S. *J. Phys. Chem. B* **2011**, *115*, 6876–6884.
- (26) Jameson, C. *J. Solid State NMR* **1998**, *11*, 265–268.
- (27) Pines, A.; Gibby, M. G.; Waugh, J. S. *J. Chem. Phys.* **1973**, *59*, 569–590.
- (28) Stejskal, E. O.; Schaefer, J.; Waugh, J. S. *J. Magn. Reson.* **1977**, *28*, 105–112.
- (29) Dixon, W. T. *J. Chem. Phys.* **1982**, *77*, 1800–1809.
- (30) Fung, B. M.; Khitrin, A. K.; Ermolaev, K. *J. Magn. Reson.* **2000**, *142*, 97–101.
- (31) Bloch, D. R. *Polymer handbook*; John Wiley: New York, 1999.
- (32) Wunderlich, B. *Thermal Analysis*; Academic Press: New York, 1990.
- (33) Look, D. C.; Lowe, I. *J. Chem. Phys.* **1996**, *44*, 3441–3452.
- (34) Press, W. H.; Teukolsky, S. A.; Vetterling, W. T.; Flannery, B. P. *Numerical Recipes in C: The Art of Scientific Computing*, 2nd ed.; Cambridge University Press: Cambridge, U.K., 1992.
- (35) Liu, J.; Yee, A. F. *Macromolecules* **2000**, *33*, 1338–1344.
- (36) Li, X.; Yee, A. F. *Macromolecules* **2003**, *36*, 9421–9429.
- (37) Williams, G.; Watts, D. C. *Trans. Faraday Soc.* **1970**, *66*, 80–85.
- (38) Cumbreiro, F. L.; Sanchez-Bajo, F.; Guiberteau, F.; Solier, J. D.; Munoz, A. *J. Mater. Sci.* **1993**, *28*, 5387–5396.